JOURNAL OF THEORETICAL AND APPLIED MECHANICS
50, 2, pp. 423-440, Warsaw 2012
50th Anniversary of JTAM

NUMERICAL INVESTIGATION OF COMPRESSOR ROTOR BLADE CLOCKING EFFECTS ON AERODYNAMIC LOADING OF THE STATOR VANE

Pei-Gang Yan

School of Energy Science and Engineering, Harbin Institute of Technology, Harbin, China

Xiao-Qing Qiang, Zhao-Hui Du

School of Mechanical Engineering, Shanghai Jiao Tong University, Shanghai, China

e-mail: qiangxiaoqing@sjtu.edu.cn

Wan-Jin Han

School of Energy Science and Engineering, Harbin Institute of Technology, Harbin, China

The unsteady flow fields of a three-stage axial compressor are simulated. The 3D N-S equations are solved by using the frequency domain transformed method based on the harmonic function. The main efforts are focused on the effects of the second stage rotor blade clocking configuration on aerodynamic loading of the stator vanes. The unsteady aerodynamic loadings of each blade row are analyzed in time and frequency domains. The results point out that the aerodynamic loading of the middle stage stator vane is significantly affected as the rotor blades changing with different clocking configuration. At CLK0 configuration, the middle stage stator vane is affected by the aerodynamic force whose direction is sometimes reverse with the regular force. At CLK2 configuration, the aerodynamic force of the stator vane is always positive and the fluctuation amplitude is smaller than those of other configurations. Meanwhile, the response of stator vane S2 to one blade passing frequency (BPF) is minimum comparing to others.

Key words: compressor, unsteady flow, clocking effect, flow exciting force

Nomenclature

$U, \overline{U}, U'$ – conservation variable, time-averaged and disturbance conservation variable, respectively, [-]

N_F, N_{fou} – harmonic disturbance and Fourier series number, [-]

L – lower boundary in tangential direction, [-]

B – blade chord length, [m]

f – frequency, [Hz]

F – aerodynamic force, [N]

M – aerodynamic moment, [Nm]

A – disturbance amplitude, [-]

ω – disturbance frequency, [Hz]

T – period, [-]

C_p, C_F, C_M – coefficient of static pressure, aerodynamic force and aerodynamic moment, [-]

γ – aerodynamic force angle, [deg]

P, P_0, P_0^* – local static pressure, static and total pressure at inlet, [Pa]

Superscripts and subscripts: x – compressor axial direction, y – component perpendicular to blade, cg – center of gravity.

1. Introduction

The unsteady flow in a gas turbine has an important effect on its performance parameters. As the design system expand to account for these interactions, a better understanding of the underlying unsteady flow mechanism is necessary for accurate assessing of the performance and reliability of the gas turbine (Nicole *et al.*, 2010). Due to excessive stress caused by blade vibration, the blades of a gas turbine can occur damaged. The main factors that affect blade stress are the feature of blade vibration and unsteady flow characteristics of the flow exciting force (Jia and Vogeler, 2007). Therefore, to ensure the blades have a good vibration feature and to control the aerodynamic force is an effective method for reducing blade stress. The accident rate of the blade can be reduced effectively by controlling the flow of exciting force and the life cycle also would be extended (Srivastava *et al.*, 2003).

Many researches have been carried out to investigate the clocking effect on the mechanism of the development and the loss feature of the boundary layer in the compressor, as well as its effect on the compressor stage performance. Computational efforts are devoted to the efficiency variations associated with the stator vane clocking configurations (Zhou X. and Zhou S., 2009). It can be concluded that the maximal efficiency is obtained when the wake of the

upstream stator blade row impinges the blade leading edge of the downstream stator vane. Vice versa, the minimal efficiency is associated with the wake passing the mid-vane passage. Some simulations point out a difference in the stator vane performance when the wake of upstream blade transports along the pressure surface versus the suction surface of the downstream blade in their reference (Li *et al.*, 2007). The interactions of both wake/shock and wake/boundary layer are discussed in detail (Soranna *et al.*, 2008), which point out that the stator vane clocking could provide possible environment to improve performance by modifying unsteady blade row interactions.

Unfortunately, on one hand, these works mainly focus on the stator vane clocking and its effect on aerodynamic design. On the other hand, most of these researchers explore their studies mainly by an experimental method. When a numerical calculation is carried out, the count of each blade row is usually compelled to be scaled, which has always been a difficulty in unsteady flow computation of turbo machinery and could not be directly used for practical problems. In the three middle stages of a certain axial compressor studied in this paper, when the rotor blades are at different circumferential indexing, the stator vane suffers significantly different aerodynamic loading, and even occur broken. Therefore, this paper takes efforts on the clocking effect of rotor blades. The effective numerical method of unsteady flow field calculation is investigated. The feature of the flow exciting force is analyzed. The model of aerodynamic force is established to explore the relationship of the aerodynamic force with the clocking configuration of rotor blades. In this paper, both the aerodynamic and strength characteristics are considered, which is aimed to provide an engineering design basis for compressor stages of the gas turbine system.

2. Numerical method

The harmonic method is an efficient nonlinear numerical method, especially suitable to unsteady numerical solution of multi-stage axial flow turbo machinery (Ekici *et al.*, 2010).

By using the harmonic method, the flow variables to be solved are decomposed into time averaged variables and unsteady disturbance variables, and the governing equations are transformed from the time domain to the frequency domain. In this way, the original unsteady governing equations based on the time and space are transformed into a steady governing equations based on the frequency. Since the unsteady problem is converted into steady problem,

then the computation time is greatly reduced. The most important, the blade count of each blade row could be remained unchanged.

For the research model of this paper, the harmonic method does not require adjusting the blade counts of all blade rows, and does not need to store the data in the flow field of multiple space positions. It only requires computer storage space several times greater than that needed for steady calculation. So the harmonic method is an effective and feasible way for solving the current problem.

2.1. Governing equations

The numerical method adopts a series of modules of FINE$^{\mathrm{TM}}$/Turbo software package developed by NUMECA.

The basic governing equations of the unsteady flow are as follows

$$\begin{aligned}\frac{\partial}{\partial t}\iiint U\ dVol + \iint (Fn_x + Gn_\theta + Hn_r)\ dA \\ \iiint S\mathrm{i}\ dVol + \oint \int (Fvn_x + Gvn_\theta + Hvn_r)\ dA\end{aligned} \tag{2.1}$$

Decompose the conservation variables into time average ones, and a group of multi-harmonic disturbance variables are

$$U = \overline{U} + \sum_{n=1}^{N_F} U'_n \mathrm{e}^{-\mathrm{i}n\omega t} = \overline{U} + \sum_{n=1}^{N_F}\sum_{n=1}^{N_{fou}} [A_{in}\sin(\mathrm{i}\omega_n t) + B_{in}\cos(\mathrm{i}\omega_n t)] \tag{2.2}$$

The time-averaged equation and perturbation equations are then obtained:

— time-averaged equation

$$\iint (\overline{F}n_x + \overline{G}n_\theta + \overline{H}n_r)\ dA = \iiint \overline{S}\mathrm{i}\ dVol + \oint \int (\overline{F}vn_x + \overline{G}vn_\theta + \overline{H}vn_r)\ dA \tag{2.3}$$

— unsteady disturbance equations

$$\begin{aligned}\iiint -\mathrm{i}\omega U'\ dVol + \oint \int (F'n_x + G'n_\theta + H'n_r)\ dA \\ \iiint S'\mathrm{i}\ dVol + \oint \int (F'vn_x + G'vn_\theta + H'vn_r)\ dA\end{aligned} \tag{2.4}$$

The second order central difference scheme is applied to the spatial discretization of the equations, and the S-A turbulence model is utilized.

2.2. Boundary conditions

For the time-averaged equation, the total temperature, the total pressure and flow angle are given at the inlet, and the back pressure is given at the outlet. At the rotor/stator interface, the 2D non-reflecting boundary conditions are utilized.

For the disturbance equations, the phase-lagged boundary condition is given

$$(U')^U = (U')^L \mathrm{e}^{\mathrm{i}\sigma} \tag{2.5}$$

where σ is the phase angle between blade rows, U and L represents the circumferential flow variables along the upper and lower boundary, respectively. In the treatment of the rotor/stator interface, the downstream and upstream of the interface adopt the 2D non-reflecting boundary conditions.

At the inlet of the interface, the incoming wake perturbations in terms of velocities, pressure and density are produced by the spatial Fourier transform of the time-averaged non-uniform field at the upstream outlet. At the outlet of the interface, the potential disturbances are produced by the spatial Fourier transform of the time-averaged non-uniform field at the downstream inlet.

Since the higher order of the harmonic decomposing, the more numbers of the harmonic solution, and the calculation have corresponding higher accuracy, then there is an excessive computer memory requirement for applying the harmonic method.

2.3. Validation of steady calculation method

The validation is carried out by comparing the experimental data with the steady numerical results. The experiments were performed in the high-speed compressor test rig at Harbin Institute of Technology. The three-dimensional numerical simulation of the fan stage is demonstrated by using the commercial CFD software FINE/TURBO.

The spatial discretization meshes (Fig. 1) of rotor blades and stator vanes flow passage for the fan stage are generated by pre-processing module IGG/AutoGrid.

The first cells of the computational mesh near the blade wall and end wall meet $y^+ < 3$, the total number of computational mesh nodes shown in Fig. 1 is about 500 000. The comparison of computational results of the isentropic efficiency and the pressure ratio with the experimental results is shown in Fig. 2.

It is shown that there are differences between the flow ranges of the numerical simulation speed line and the experimental measurement in some extent,

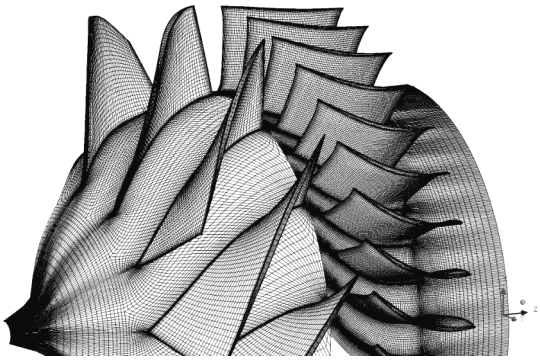

Fig. 1. Computational mesh of the fan stage

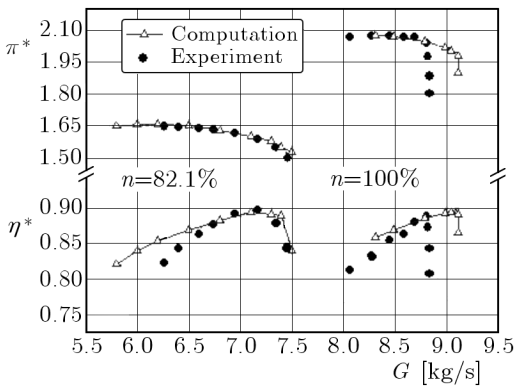

Fig. 2. Comparison of the experimental results with the numerical ones

but the difference is mainly at the low flow rate points, and on the whole, the numerical results are in good agreement with the experiment data. The following research focus on the operating condition.

2.4. Unsteady calculation method validation

The blade scaling method has been widely used in turbo machinery unsteady flow field calculation. On the condition that the upstream and downstream blade counts are reasonable scaled, the results of this method have high credibility.

In order to further investigate the reliability of the unsteady harmonic method, take the blades of the middle three stages for a heavy duty gas turbine compressor as the research subject (Fig. 3). Firstly, the count of blades is scaled as Table 1 shows, and then the harmonic method and the scaling

method are respectively used to the calculation of the 2D unsteady flow field. The differences of the results calculated by these two methods are identified. Figure shows the computational mesh.

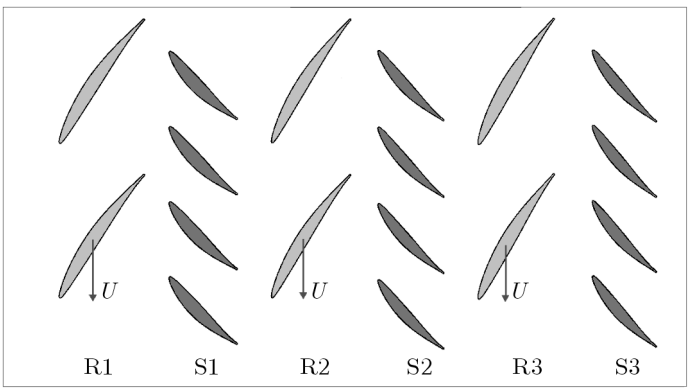

Fig. 3. Compressor blade configuration

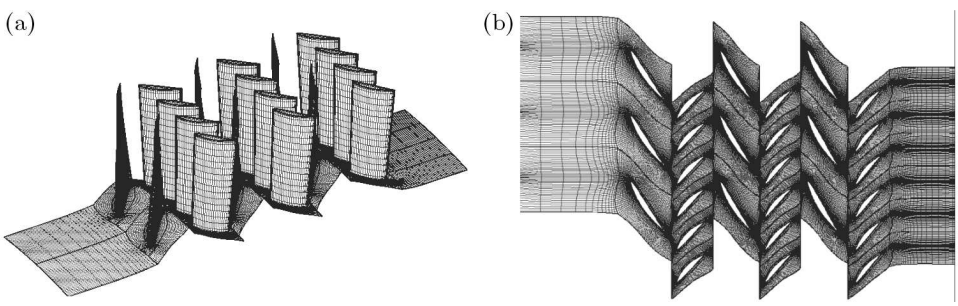

Fig. 4. Computational mesh; (a) 3D mesh, (b) grid topology at the mid-span

Table 1. Scaled blade count of the three-stage compressor

Blade	R1	S1	R2	S2	R3	S3
Count	64	128	64	128	64	128

In the process of calculation, the inlet boundary conditions are given as: total temperature 657.18 K, total pressure 1.252 kPa and the circumferential flow angle 38.17°. The average static pressure, considering the radial balance equation, is given at the outlet. It increases from 1200kPa to 1750 kPa, where the static pressure at the design point is 1520 kPa. Its corresponding mass flow is 625 kg/s with the design rotational speed 3000 rpm

$$Cp = \frac{P - P_0}{P_0^* - P_0} \tag{2.6}$$

where P represents the local static pressure, P_0 is the averaged static pressure at the inlet of the rotor blade cascade, P_0^* is the averaged absolute total pressure at the inlet of the stator vane, and is the averaged relative total pressure at the inlet of the rotor blade cascade.

Figure 5 shows the entropy transportation contour obtained by the harmonic method and the scaling method. Figure 6 shows the time-averaged and fluctuation values of the blade profile pressure obtained by these two methods.

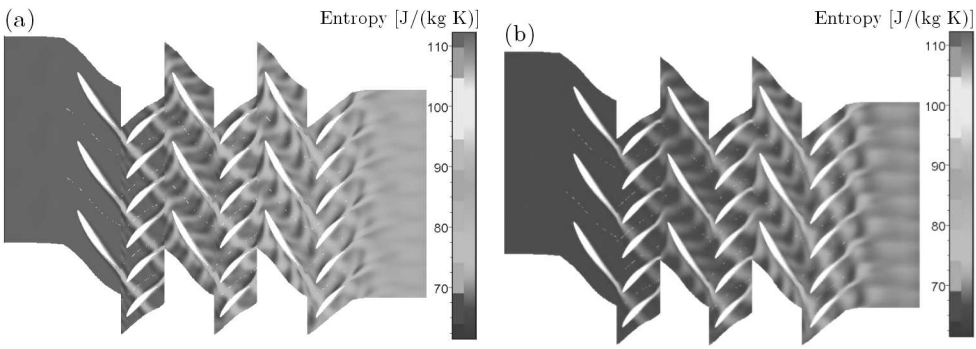

Fig. 5. Entropy transportation contour; (a) harmonic method, (b) scaling method

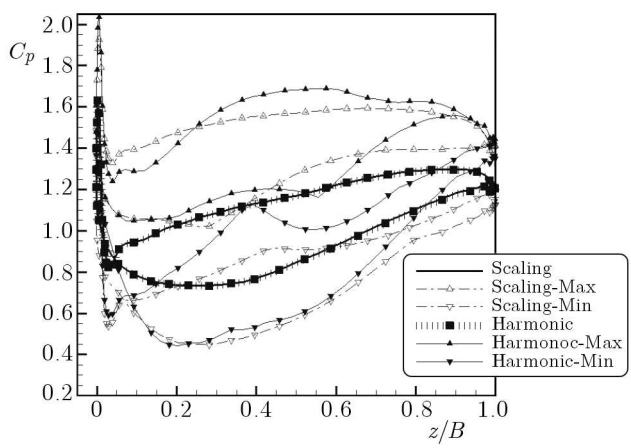

Fig. 6. Time-averaged and fluctuation value of C_p

From Fig. 5 it can be observed that on the transfer surfaces of each row blade, the entropy distributions calculated by the harmonic method are basically

continuous. It is shown that the harmonic method has a high computational accuracy in the unsteady calculating rotor/stator transfer aspects.

Meanwhile, focusing on the S2 blade surface static pressure, it is observed that in one period the unsteady fluctuations of the static pressure calculated by the harmonic method are higher than those calculated by the scaling method, but the difference is not significant. Both time-averaged curves of the static pressure calculated by these two methods are fully in line, so the results of aerodynamic forces and moments calculated by the harmonic method blade are reliable.

3. Computational results and analysis

Taking into account of the middle three stages of the gas turbine compressor as the research subject, without changing the blade count of each blade row, this paper will investigate the rotor blade clocking effects on the aerodynamic loading of the stator vane.

Figure 7 shows the model and four different clocking configurations. The real blade count of each row is given in Table 2. Figure 8 shows the isentropic efficiency fluctuation of the whole three-stage compressor. Here, the isentropic efficiency of a multistage compressor stage is defined as

$$\eta = \frac{\left(\frac{P_2^*}{P_0^*}\right)^{\frac{k-1}{k}} - 1}{\frac{T_2^*}{T_0^*} - 1} \tag{3.1}$$

where, the subscript 0 and 2 denote the inlet and outlet of the whole stage, respectively.

Table 2. Real blade count of the three-stage compressor

Blade	R1	S1	R2	S2	R3	S3
Count	64	132	64	130	64	132

From this figure, the performance of the three-stage compressor can be seen clearly under four different CLOCKING positions of the R2 blade. Though the R2 CLOCKING has merely slight influence on the whole performance of the compressor stage, it is not enough to provide verification for the structural reliability of the compressor blade. So, it is necessary to deeply investigate the mechanism of the unsteady aerodynamic force exerted on each blade row in the following part of this paper.

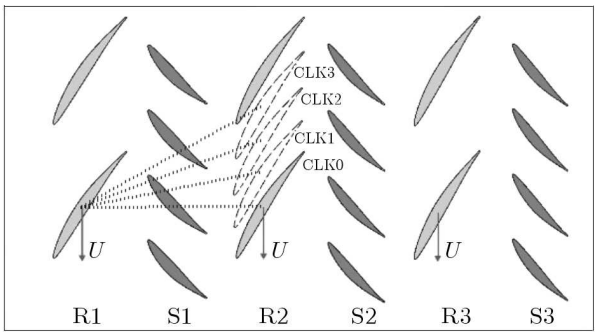

Fig. 7. Clocking configurations of the three-stage compressor

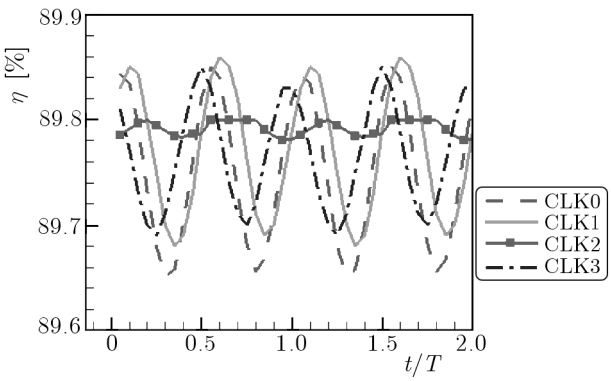

Fig. 8. Isentropic efficiency of the three-stage compressor

3.1. Analysis of entropy transportation

Figure 9 shows the entropy transportation processes when R2 is positioned in the CLK0 and CLK2 configurations respectively. The following comparative analysis is to consider transient results at a specified time.

When R2 is positioned at CLK0 configuration, the wake and potential flow of R1 transports to flow passage of S1, the acceleration process of flow near S1 blade suction surface makes the wake stretched, the role of the boundary layer of the stator vane makes the wake twisted, but the flow under adverse pressure gradient has no significant dissipation.

Looking at the picture, we can notice that there is an important phenomenon occurring when R2 is positioned at CLK0 configuration. That is the wake of R1 and the part of the wake of S1 just transported to the leading edge of R2 after mixing at the trailing edge of S1, and in a period they are always cut by the leading edge of R2. Therefore, the wake of R1 is mainly dissipated in

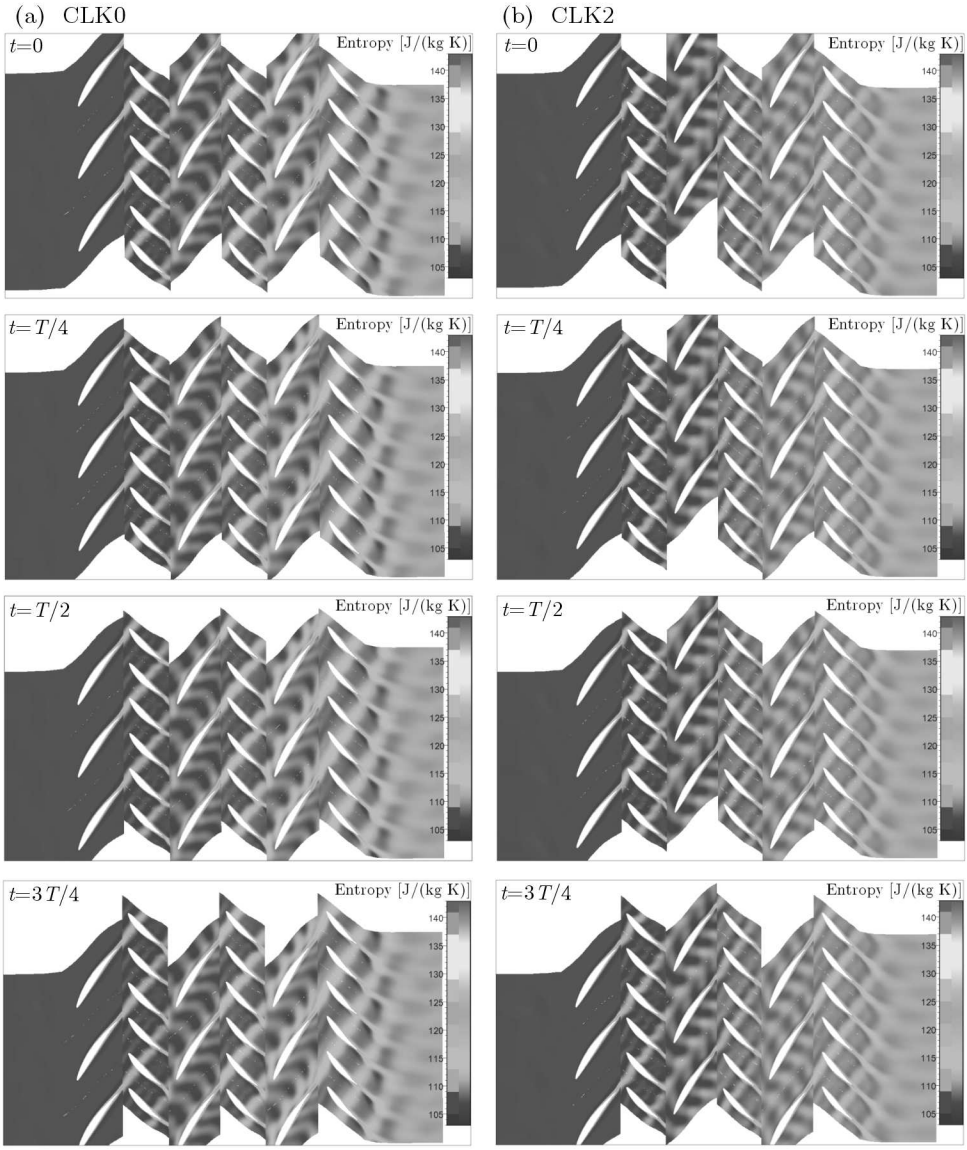

Fig. 9. The entropy transportation contour; (a) CLK0, (b) CLK2

the boundary layer of R2. On the suction surface of R2, part of the wake of R1 mixes with the wake of S1 to form the wake of R2, continuing to transport to downstream areas. Thus, the entropy transportation of S2 mainly as a single strong wake constantly being cut, is accumulated and dissipated in the downstream. When R2 is positioned at CLK2 configuration, the part of

the wake of R1 and the wake of S1 enter into the middle of R2 flow passage after mixing, and transport to the outlet of R2. The leading edge of R2 cut the wake and potential flow of S1 alternatively. As at the outlet of R2 there are wakes of both R1 and S1, so the entropy transportation of S2 reflects the transporting processes of several wakes.

Compared with that of the CLK0 configuration, the intensity of several wakes is reduced, and the twist and deformation of the wake in the transporting process are weakened. Thus the wake of R2 passing S2 directly flows into the middle of the flow passage of R3.

From the above analysis, it can be seen that when R2 at different clocking configurations is associated with different wake transportation characteristics, it results in the interaction between potential flows, and the wake and the boundary layer is significantly different. Therefore, the fluctuations of pressure caused by the wake and potential flow must lead to the fluctuation of the unsteady aerodynamic loading on the blade.

Through analyzing the transporting process of the wake and potential flow in the transient flow field, further investigation of the unsteady aerodynamic force and moment on the blade will help one to understand the mechanism of the flow exciting force on the three-stage blades.

3.2. Time domain analysis of the unsteady aerodynamic loading of the blades

In order to investigate the clocking effects of R2 on the aerodynamic loading of S2, the unsteady fluctuation amplitude and frequency of the aerodynamic force, the coefficient of aerodynamic moment and the directional angle of aerodynamic force are all analyzed in the time domain for R2 positioned at different clocking configurations.

The aerodynamic loadings exerted onto the blade are analyzed in the reference coordinate system shown in Fig. 10, in which x denotes the axial direction of the compressor and y denotes the tangential direction of rotation. The aerodynamic force is calculated by integrating the profile pressure distribution. The force angle γ represents the angle between the total and the axial force. The blade gravity center is specified with (x_{cg}, y_{cg}), so the force multiplied by the distance between the acting point and gravity center obtains the moment M. The positive direction of M is specified by the right-hand rule, which neglects the influence of viscous shear stress within the blade boundary layer.

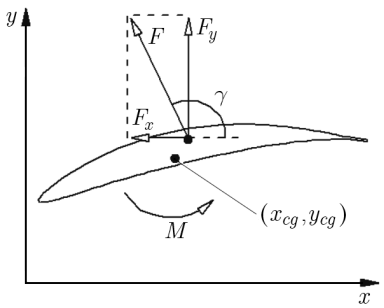

Fig. 10. Schematic view of force definition

The following expressions show the variables above

$$\begin{aligned}
&\vec{F}(t) = \vec{F}_x(t) + \vec{F}_y(t) \\
&\overline{F}_x(t) = -\Delta h \oint_L P(t)\, d\overline{y} \qquad\qquad \overline{F}_y(t) = \Delta h \oint_L P(t)\, d\overline{x} \\
&\overline{M}(t) = \Delta h \left(\oint_L P(t)(x - x_{cg})\, d\overline{x} + \oint_L P(t)(y - y_{cg})\, d\overline{y} \right) \\
&\gamma = \arctan \frac{\overline{F}_y}{\overline{F}_x} \qquad C_F = \frac{F(t)}{\overline{F}} \qquad C_M = \frac{M(t)}{\overline{M}}
\end{aligned} \tag{3.2}$$

where $F(t)$ and $M(t)$ represents the transient aerodynamic force and moment on the blade profile, respectively. $P(t)$ represents the transient pressure of a discrete point on the blade profile. C_F and C_M denote the coefficient of the force and moment, respectively.

Figure 11 shows the variation of the aerodynamic loading of S2 with time. The two components of the aerodynamic force are all negative during the period of 0-0.3T when R_2 is positioned at CLK0. In addition, the direction of the aerodynamic force angle is in the fourth quadrant at this transient time. It indicates that during that time period, the pressure on the suction side of the blade is higher than that on the pressure side, and the force is in the reverse direction of the regular pointing from the suction surface to the pressure surface. A similar phenomenon also occurs at both CLK1 and CLK3 configurations.

The aerodynamic loading of S2 is always positive in one period when R2 is positioned at CLK2 configuration, and the fluctuations amplitude of the aerodynamic force are significantly smaller than in the other three configurations. The fluctuation range of directional angle of the aerodynamic force is

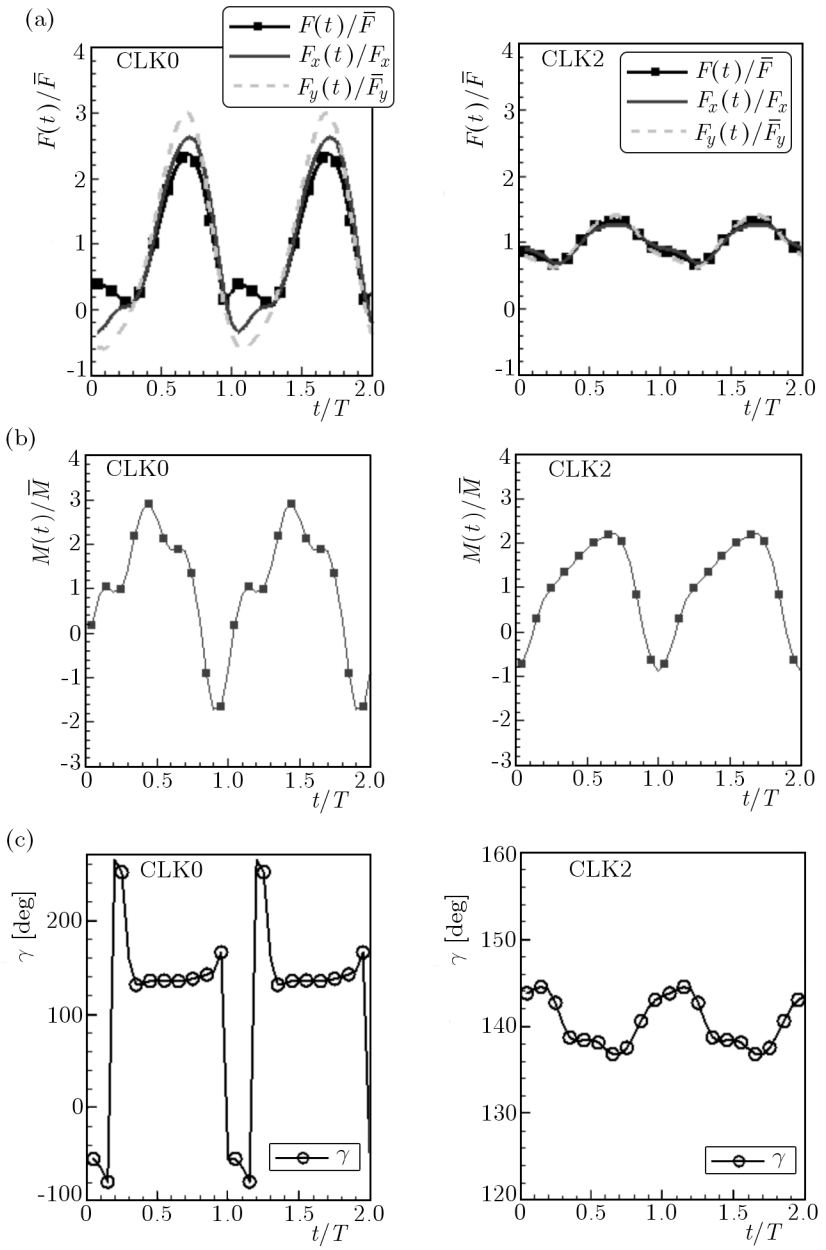

Fig. 11. Unsteady aerodynamic loadings of S2; (a) aerodynamic force, (b) aerodynamic moment, (c) directional angle of the aerodynamic force

also smaller. It indicates that at CLK2 configuration, S2 has more stable aerodynamic loading, which is less disturbed by the wake and the potential flow, and this is consistent with the preceding analysis of the wake transportation.

It is noteworthy that at CLK2 configuration the fluctuation amplitude and frequency of the aerodynamic moment are smaller than those in the other clocking configuration, which is conducive to extend the fatigue life of S2 blade.

3.3. Frequency domain analysis of the unsteady aerodynamic force of the blades

In order to obtain the information about the disturbance of each blade row in the frequency domain, the FFT (Fast Fourier Transform) to the unsteady aerodynamic force on the blade are implemented. Here is the definition of the frequency of blade rotation speed: the product of the blade count and the rotational speed.

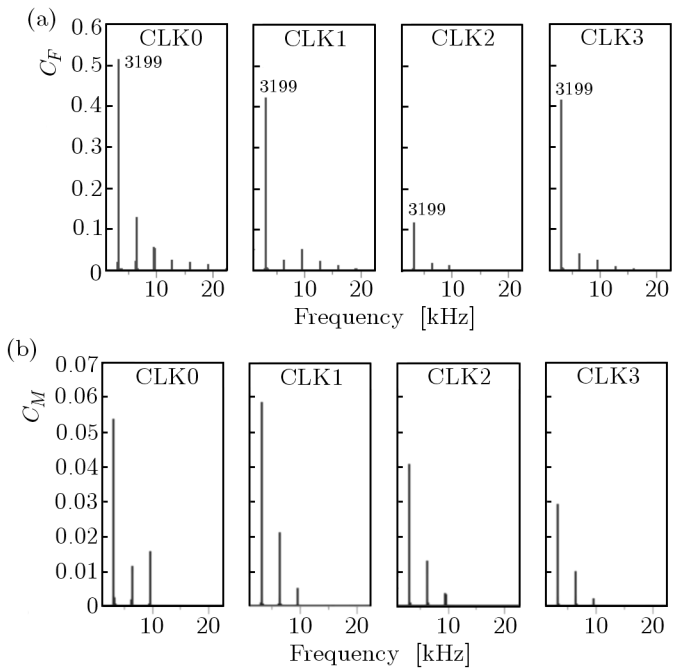

Fig. 12. Frequency spectra of the unsteady aerodynamic loadings of S2 blade; (a) coefficient of aerodynamic force, (b) coefficient of aerodynamic moment

Figure 12 shows the frequency spectra of S2 aerodynamic force and aerodynamic moment for R2 positioned in the four different clocking configurations. The 1BPF amplitudes of the aerodynamic force are 52%, 43%, 13% and

42%, respectively. The 2BPF and 3BPF amplitudes of the aerodynamic force are 13% and 5% when R2 is positioned at CLCK0 configuration. The 1BPF amplitudes of the aerodynamic moment are 53%, 58%, 41% and 30%, respectively. The 2BPF amplitudes of the aerodynamic moment are 11 %, 20%, 12% and 10%.

It can be found that the circumferential indexing of R2 significantly affects the 1BPF amplitudes and the aerodynamic loading of S2. When R2 is positioned at CLK2 configuration, the 1BPF amplitude is smaller than that at CLK0 and CLK1 configurations. Although the 1BPF amplitude of the aerodynamic moment is higher than CLK3, S2 suffers changes in the unsteady aerodynamics and is more stable. The changing number of the aerodynamic moment is less, so the blade aerodynamic loading is significantly lower than that at CLK3.

As the weakest frequency response of the aerodynamic loading on the blade has the smallest amplitude, the frequency spectra can be used to further illustrate that at CLK2 configuration, R2 has minimal impact on S2, and at CLK0 configuration, S2 blade most likely endures fatigue damage.

4. Conclusions

Through the above analysis, the following conclusions can be obtained:

- Under unsteady conditions, there are significant disturbances between the blade rows, which mainly comes from the alternating influences of the wake and potential flow on the blade rows. The wake and potential flow of the upstream blade row not only affect the adjacent blade row downstream, even also cause disturbance to farther downstream blades. In the process of wake transportation within the flow passage of the downstream blade, the disturbance of the wake and potential flow will cause that the amplitude and phase of the aerodynamic force circumferential component and the axial component significantly change, thus the alternation of the wake and potential flow is the main reason for the unsteady aerodynamic loading on the blade.

- Different clocking positions correspond to different entropy transportation characteristics. When R2 is positioned at CLK0 configuration, the wake of R1 and a part of the wake of S1 are just transported to the leading edge of R2 after mixing at the trailing edge of S1, and in one period

they are always cut by the leading edge of R2. The entropy transportation of S2 is mainly the wake transporting process of R2 wake. When R2 is positioned at CLK2 configuration, the part of the wake of R1 and the wake of S1 enter the middle segment of R2 flow passage after mixing, and then transport to the outlet of R2. The leading edge of R2 cuts the wake and potential flow of S1 alternatively. The entropy transportation of S2 reflects the transporting processes of multiple wakes.

- The spectral analysis of the aerodynamic loading on S2 shows that when R2 is at CLK0 configuration, the aerodynamic force exerted on S1 is reverse to the regular force in a part of one period, and in the meantime, the aerodynamic force and moment have maximum fluctuation amplitudes. While at CLK2 configuration, the aerodynamic force direction on the stator vane is always positive, the fluctuation amplitude is also smaller than those of other configurations, and the fluctuation amplitude of the aerodynamic moment, and the number of times of changing its direction is also smaller, which helps one to reduce the negative impact on S2 blade.

Acknowledgements

This work was supported by the National Natural Science Founding of PR China under Grant No. 50706009.

References

1. Ekici K., Hall K., Kielb R., 2010, Harmonic balance analysis of blade row interactions in a transonic compressor, *Journal of Propulsion and Power*, **26**, 2, 335-343

2. Jia H., Vogeler K., 2007, Effect of clocking on the unsteady rotor blade loading in a 1.5 stage low-speed axial compressor, *Proceedings of ASME GT2007*, GT2007-27237

3. Li S., Su J., Feng G., Wang Z., 2007, Study of performance and profile pressure distribution of transonic compressor under rotor-stator interaction condition, *Journal of Aerospace Power*, **22**, 7, 1153-1160

4. Nicole L.K, Patrick B.L, Sanford F., 2010, An experimental study of vane clocking effects on embedded compressor stage performance, *Journal of Turbomachinery*, **132**, 1, 1-10

5. Soranna F., Chow Y.C., Uzol O., Katz J., 2008, The effects of IGV wake impingement on the boundary layer and the near-wake of a rotor blade, *Proceedings of ASME GT2008*, GT2008-50598

6. Srivastava R., Bakhle M.A., Keith Jr. T.G., 2003, Numerical simulation of aerodynamic damping for flutter analysis of turbomachinery bladed rows, *Journal of Propulsion and Power*, **19**, 2, 260-267

7. Zhou X., Zhou S., 2009, Investigation of the effect of wake impact effect on vortex sheets of the downstream blade row in axial compressor, *Journal of Aerospace Power*, **24**, 3, 608-614

Analiza numeryczna wpływu wzajemnego ustawienia łopat sprężarki na obciążenie aerodynamiczne kierownicy

Streszczenie

Praca zawiera wyniki symulacji numerycznej nieustalonego pola przepływu w trójstopniowej sprężarce osiowej. Trójwymiarowe równania Naviera-Stokesa rozwiązano metodą transformacji w dziedzinie częstości opartej na funkcji harmonicznej. Główny wysiłek włożono w badania wpływu konfiguracji łopat kierownicy i wirnika drugiego stopnia sprężarki na obciążenie aerodynamiczne kierownicy. Obciążenie to o charakterze nieustalonym przeanalizowano dla każdego rzędu łopatek w dziedzinie czasu i częstości. Wyniki wykazały, że obciążenie aerodynamiczne kierownicy środkowego stopnia sprężarki znacząco zależy od wzajemnego ustawienia łopat wirnika i kierownicy. Dla konfiguracji oznaczonej CLK0 kierownica podlega obciążeniu siłą, której zwrot bywa przeciwny do kierunku typowego w przypadkach regularnych. Natomiast konfiguracją CLK2 generuje zawsze dodatnią wartość siły aerodynamicznej, której fluktuacje amplitudy są jednocześnie mniejsze niż w innych konfiguracjach. Ponadto stwierdzono, że wrażliwość aerodynamiczna łopaty kierownicy S2 na częstotliwość łopatkową (BPF) jest minimalna w stosunku do innych konfiguracji.

Manuscript received June 13, 2011; accepted for print July 18, 2011